ACCEPTED MANUSCRIPT

SOL width broadening by spreading of pedestal turbulence

To cite this article before publication: Xu Chu *et al* 2022 *Nucl. Fusion* in press https://doi.org/10.1088/1741-4326/ac4f9f

SOL Width Broadening by Spreading of Pedestal Turbulence

Xu Chu[1,4], **P. H. Diamond** [2*], **Zhibin Guo** [3]

[1]School of Engineering Science, Univeristy of Chinese Academy of Sciences, Beijing, People's Republic of China
[2]Department of Physics, University of California San Diego, La Jolla, CA, United States of America
[3]School of Physics, Peking University, Beijing, People's Republic of China
[4]Department of Astrophysics, Princeton University, Princeton, NJ, United States of America

E-mail: pdiamond@ucsd.edu
* Author to whom any correspondence should be addressed
ORCID IDs:
Xu Chu: https://orcid.org/0000-0002-0382-6428
P. H. Diamond: https://orcid.org/0000-0003-3273-2604

Abstract

The pedestal turbulence intensity required to convert the thin, laminar H-mode SOL(scrape-off layer) to a broad turbulent SOL is calculated using the theory of turbulence spreading. A lower bound on the pedestal turbulence level to exceed the neoclassical heuristic drift width is derived. A reduced model of SOL turbulence spreading is used to determine the SOL width as a function of intensity flux from the pedestal to the SOL. The cross-over value for exceeding the HD(Heuristic Drift model) width is then calculated. We determine the pedestal turbulence levels – and the critical scalings thereof – required to achieve this level of broadening. Both drift wave and ballooning mode turbulence are considered. A sensitivity analysis reveals that the key competition is that between spreading and linear $E \times B$ shear damping. The required pedestal turbulence levels scale with ρ/R.

Submitted to: *Nucl. Fusion*

1. Introduction

Perhaps the central question of magnetic fusion research today is how to reconcile good confinement with satisfactory power handling and boundary control[1]. The advent of H-mode[2] and other enhanced confinement regimes has spawned a set of new questions in the realm of of power handling. These include ELM(edge localized model) mitigation, impurity and particle control, and the SOL heat load width. The last –namely the SOL width – is the subject of this paper. The approaches to these questions all require an element of compromise, i.e. one must consider remedies which involve trade-offs between confinement and power handling, so as to optimize the overall device performance. A cost-benefit analysis approach is usually required.

One power handling issue of great importance is that of the heat load scale, set by the width of the scrape off layer(SOL). A broad SOL width is desireable, so as to accommodate the power density flowing to the plasma facing component (PFC) in the divertor. For a long time, turbulence generated locally (in the SOL) was thought to determine the SOL width via turbulent transport[3]. The picture here was analogous to the textbook example of a turbulent boundary layer, the scale of which is set by diffusion and the transit time of a parcel through the boundary layer[4][5]. However, more recent scaling studies[6] indicated this was not the case, and that the SOL width in H-mode was quite narrow, and scaled inversely with poloidal field. The heuristic drift (HD) model[7] nicely explained the observed SOL width (λ) scaling by relating the heat load width to the magnetic drift velocity $v_D \simeq \rho v_{Ti}/R$ and the ion transit time $\tau_\parallel = qR/v_{Ti}$, so $\lambda \simeq v_D \tau_\parallel \sim \epsilon \rho_{\theta_i}$. Here, ρ is the ion gyro-radius, v_{Ti} is the ion thermal velocity, q is the safety factor, ϵ is the inverse aspect ratio, ρ_{θ_i} is the poloidal ion gyro-radius. Note that here λ is seen to be small, independent of machine size, and to scale as $\sim 1/B_\theta$. The HD model is consistent with present day scalings for the SOL width in H-mode[8], though the data analysis suggests that physics other than neoclassical is at work in some cases. It also is, plainly put, bad news. In particular, both the inverse scaling with current and the independence of size are undesirable. Recent work indicates that strong $E \times B$ shear in the SOL and its concomitant stabilizing influence underpins the HD model[9], which ignores collective effects *a-priori*.

Given the situation described above, it is natural to explore possible mechanisms for broadening the SOL. Turbulence spreading from the pedestal to the SOL is a natural candidate. The idea here is to convert a laminar boundary layer to a broader, turbulent one by injection of turbulence from the pedestal into the SOL. Of course, this requires pedestal turbulence and the outward spreading thereof to drive the process. Turbulence spreading is intensively studied in fluid mechanics, as the topic entrainment – familiar in the context of free shear flows and wakes[5]. Entrainment refers to the process whereby a turbulent patch expands into stable or irrotational region of the flow. Spreading[10] is especially relevant since turbulent pedestal states are also of current interest for ELM mitigation [11] and particle and impurity control. Examples of turbulent pedestal states include "grassy ELMs"[12] – defacto states of modest MHD ballooning mode turbulence – and the wide pedestal QH-mode [11] . It is natural then to inquire if the pedestal turbulence can also resolve yet another problem, namely that of the SOL width. The aim here is to determine if spreading-induced turbulent broadening can exceed the neoclassical HD width. This requires achieving at least an R.M.S. $E \times B$ velocity in the SOL of $\tilde{v}_\perp > v_D$. As we will see, this condition also sets the required pedestal turbulence level.

It is important to emphasize that the key question here is *quantitative* . Turbulence spreading from the pedestal to the SOL is to be expected, since the free energy available in the pedestal is much larger, on account of the outward heat flux and closed core field lines. Also, there is ample direct evidence of outward spreading (i.e. from the core towards the SOL) of edge turbulence intensity. This has been ascertained by measurement of the turbulence intensity flux [13][14][15] and by calculation of the transfer entropy [16]. The latter approach uses fluctuation measurements to determine the direction of the flow of information carried by turbulence spreading. All measurements indicate outward spreading. Thus, there is indeed little doubt that a sufficiently turbulent pedestal can drive spreading to broaden the SOL. The real question is whether this is possible with an acceptable degradation of confinement. Here we aim to answer precisely that question. With this goal in mind, our analysis follows in two sequential parts. The first addresses the effect of an influx of turbulence intensity on the SOL turbulence level, and thus the SOL width,

via $\tilde{v}_{\perp rms}$. The second examines what level of pedestal turbulence is required to drive the necessary SOL width broadening.

In this paper, we examine the physics of the SOL width scale, with special emphasis on $E \times B$ shear and its implications for stability, and on turbulence spreading and its impact on SOL broadening. The aim here is to determine the pedestal turbulence level required to broaden the layer beyond the HD width. First, we review the linear interchange stability of the SOL and show that $E \times B$ shear and sheath boundary conditions combine to strongly stabilize the SOL. Then, using a generalized $K - \epsilon$ model of turbulence spreading [17] [18] [19] [20] , we derive an expression for the SOL turbulence energy density e in terms of the turbulence energy density influx from the pedestal, the rate of linear damping by $E \times B$ shear, and nonlinear damping. This value of e so determined then sets the layer width as $\lambda = \left(\lambda_{HD}^2 + \tau^2 e\right)^{1/2}$. Here $\tau = L_\parallel / c_s$ is the transit time through the SOL and λ_{HD} is the HD model width. The predicted value of λ/λ_{HD} falls along two branches, with a transition region in between. $\tilde{v} \sim v_D$ is required to achieve the transition layer. We then turn to the question of what levels of pedestal turbulence are necessary for broadening. Two prototypical examples are considered, namely collisional drift wave turbulence and ideal ballooning mode turbulence. In both cases, we determine what pedestal conditions are necessary to broaden the layer. A major element in this analysis is the effect of the edge transport barrier due to the strong electric field shear in H-mode on regulating spreading[21]. The effect of shearing is accounted for via the correlation time in the spreading flux from the pedestal. In the case of collisional drift waves – representative of pedestal microturbulence, we derive a lower bound on pedestal fluctuation levels sufficient for SOL layer broadening. For ballooning mode turbulence – representative of Grassy ELMs – we show that only a small exceedance of the ideal marginality condition is sufficient to produce the requisite layer broadening. Thus, we demonstrate that a state of quasi-marginal ballooning mode turbulence – equivalent to a Grassy ELM state – can support a SOL width which exceeds the HD prediction. A sensitivity study of our result to the various parameters in the nonlinear damping model is presented, as well. We show that the key competition at the transition is that between the spreading flux and linear $E \times B$ shear damping.

The remainder of this paper is organized as following. Section 2 presents necessary background – the HD model – and explains why it works. Section 3 determines the SOL width as a function of turbulence energy influx from the pedestal and SOL parameters. Section 4 links the above-mentioned energy influx to pedestal turbulence. Two cases – namely microturbulence and ballooning mode turbulence – are examined. Section 5 presents the sensitivity studies. Section 6 gives discussion and conclusions. Several suggestions for physical and numerical experiments are presented.

2. Background: The HD Model and why it works

This section presents a brief discussion of background. Goldston, et. al. [7] proposed a heuristic drift model for the SOL heat load width which is a good fit to data [22] of present day H-mode discharges. It combines the magnetic drift velocity with the parallel transit time in the SOL to obtain a SOL width scale $\lambda \sim \epsilon \rho_\theta$, as illustrated by Fig. 1. This model is based entirely on drifts, and turbulence is not considered. However, fluctuations are observed in SOL experiments[23]. Therefore, it's natural to ask: what's the role – if any – of turbulent transport in determining the SOL width and why does Goldston's model work? In this section, we answer this question by a stability analysis of the SOL.

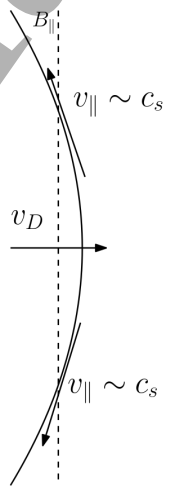

Figure 1: Cartoon of the Physics of Heuristic Drift Model. The curve represents a field line in SOL

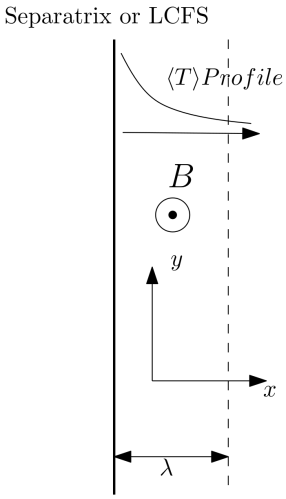

Figure 2: Geometry of the 2D fluid model for SOL

Here, a reduced electrostatic 2D model for a

sheath-connected SOL [24] is used.

$$n\frac{d\Delta_\perp\phi}{dt} = \alpha\ nT^{0.5}\left(1-e^{-(\phi-\phi_0)/T}\right) - \beta\partial_y p + n\nu_c\Delta^2\phi \quad (1)$$

$$\frac{d}{dt}n + \alpha\ T^{0.5}n = D_c\Delta_\perp n \quad (2)$$

$$\frac{d}{dt}T + \alpha_T T^{1.5} = \chi_c\Delta_\perp T \quad (3)$$

In this model, all the fields are functions of x, y, with the coordinate along the field line averaged out. ϕ is the field line averaged electrostatic potential, n is the field line averaged density. T is the field line averaged electron temperature. Ion temperature is assumed to be the same. The equations are dimensionless. The reference values for n, T are the values of those at the separatrix n_0, T_0. The reference potential is chosen as T_0/e The reference time scale is chosen as the inverse of the gyro-frequency at the separatrix $\tau_0 = 1/\omega_c$, $\omega_c = \frac{eB}{m_i}$ The reference length scale is chosen as the gyro-radius at the separatrix $rho_s = c_s/\omega_c$ where $c_s = \sqrt{(T_e+T_i)/m_i}$

The geometry of the model is illustrated in Fig. 2. ϕ_0 is the floating potential, α is the coefficient describing sheath resistivity. β is the coefficient describing magnetic curvature. S_E is the sheath energy transmission coefficient, as introduced in the model[24]. ν_c, D_c, χ_c are the neoclassical kinematic viscosity coefficient, diffusion coefficient, and heat conductivity. The neoclassical transport is assumed to be in the plateau regime, which is most relevant to experiments for the SOL. The notations are explained below:

$$d/dt = \partial_t + [\phi, \_] = \partial_t + \partial_x\phi\partial_y - \partial_y\phi\partial_x \quad (4)$$

$$\alpha_T = \alpha S_E \quad (5)$$

$$\alpha = 2\rho_s/L_\parallel \quad (6)$$

$$\beta = 2\rho_s/R \quad (7)$$

$$\phi_0 = -3T \quad (8)$$

$$L_\parallel = qR \quad (9)$$

Here, due to the floating potential in the sheath boundary condition Eq. 8, the electrostatic potential is directly linked to the temperature profile, and thus to the SOL width. As a result, the average dimensionless $E\times B$ shearing rate $\omega_s = \overline{\partial_x^2\phi} \approx \overline{\partial_x^2\phi_0} = 3T_{sep}/\lambda^2$ is large for small SOL width, and so leads to strong shear stabilization in that limit.

Now, we investigate the linear stability of this system numerically by finding the eigenvalue with maximal real part for a linear perturbation of the system. The mean $\langle n\rangle, \langle T\rangle, \langle\phi\rangle$ profiles are assumed to decay exponentially in radius as $\langle T\rangle = T_{sep}e^{-x/\lambda_T}$. The width of the density, temperature and potential profile should roughly be comparable, and are denoted by λ_n, λ_T, λ_ϕ respectively, so $\lambda_n \approx \lambda_T \approx \lambda_\phi$. At the both boundaries ($x = 0$ and $x = \infty$), all fluctuations are assumed to be zero, and so is the velocity fluctuation (derivative of the potential fluctuation). The results for the growth rate as a function of layer width are presented in Fig. 3. Note that for $\lambda \gg \lambda_{HD}$, instability occurs, because the $E\times B$ shear stabilization effect weakens as $\sim 1/\lambda^2$. Of course, at $\lambda/\lambda_{HD} \gg 1$, local instability in the SOL returns.

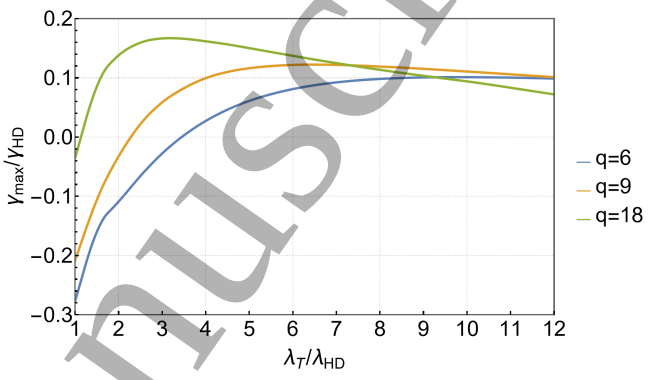

Figure 3: Maximal Linear Growth Rate of Interchange Mode in the SOL v.s. normalized pedestal width λ_T/λ_{HD} at different SOL safety number q (with $\beta = 0.001$)

Here, the normalized maximal growth rate is plotted against the normalized SOL width λ_T/λ_{HD}. The $\langle n\rangle, \langle T\rangle, \langle\phi\rangle$ are assumed to have the same shape. β is taken to be 1/1000. γ_{HD} is the ideal interchange growth rate at λ_{HD}: $\gamma_{HD} = c_s/\sqrt{\lambda_{HD}R}$. The results shows that in a relevant range of edge q from (3 to 6), the SOL is stable when the SOL width is $\sim \lambda_{HD}$, on account of the combination of large $E\times B$ shearing and sheath resistivity. This explains how HD scaling can work – there is no strong local instability in the H-mode SOL, so turbulent transport is not produced there. The origin of any fluctuations observed in the SOL must necessarily be non-local – i.e. consequence of spreading from elsewhere or the consequence of a nonlinear growth process. The latter is beyond the scope of this paper. As a result, if we are to consider the possibility of broadening the SOL width by turbulent transport, spreading of turbulence from the pedestal into the SOL should be examined.

3. SOL-Edge Connection I

Intuitively, we expect that turbulence in the pedestal should be able to broaden the SOL by turbulence spreading. It is crucial to determine how much pedestal turbulence is needed to cause significant broadening of the SOL, since excessive pedestal turbulence will result in unacceptable confinement degradation.

This problem is intrinsically one of benefit (SOL broadening) vs. cost (confinement degradation due to turbulence spreading).

In this and the next section, we study the influence of spreading on the H-mode SOL in the context of a 2-Box model , illustrated by Fig. 4. Note that the presence of the shear layer and the edge transport barrier here defines an especially clear boundary between the domains of the two boxes. As a result, the distinction between pedestal and SOL is valid. The SOL is modelled as a flux driven boundary layer with multiple drives, illustrated by Fig. 4. Apart from the usual drives – i.e. the heat flux Q and the particle flux Γ_n – a new drive, that of the turbulence intensity flux (denoted by Γ_e) from the pedestal to the SOL is included in the model. The presence of an influx of intensity makes this boundary layer problem fundamentally different from those usually encountered in textbooks. The width of the SOL is ultimately related to all these drives. The driving intensity flux is connected to the pedestal fluctuation level and pedestal parameters. This connection is discussed in the next section.

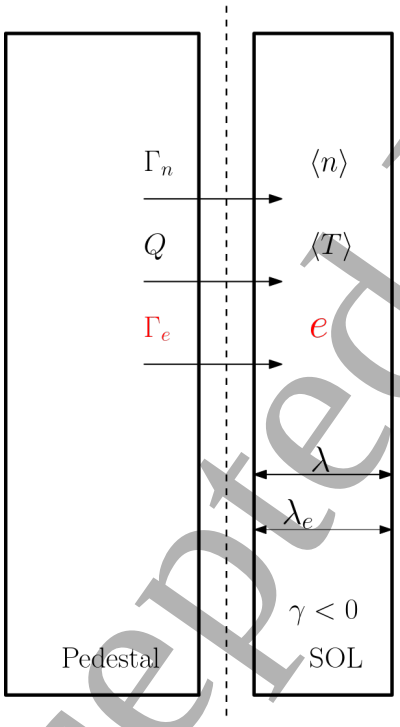

Figure 4: Illustration of Two Box Model: SOL driven by particle flux, heat flux and intensity flux (Γ_e) from the pedestal. The horizontal axis is the radial direction, and vertical axis is the poloidal direction.

Integrating Eq. 2 and Eq. 3 over the SOL, we have:

$$Q = \alpha_T \lambda_T \langle T \rangle_{sep} \tag{10}$$

$$\Gamma_n = \alpha \lambda_n \langle n \rangle_{sep} \tag{11}$$

The heat flux determines the separatrix temperature and the particle flux determines the separatrix density.

The simplest model which describes turbulence spreading is:

$$\partial_t e = \gamma\ e - \sigma\ e^{1+\kappa} - \partial_x \Gamma_e \tag{12}$$

[25][26][27]. Here, e is turbulent energy density, i.e. turbulent intensity. γ is the local linear growth rate, $\sigma\ e^{1+\kappa}$ is the nonlinear damping of the turbulence. Γ_e is the turbulent intensity flux. So, σe^{κ} is the nonlinear damping rate. Eq. 12 is generic, and is an example of a $K-\epsilon$ model, which evolves SOL turbulence energy density by linear growth γ, nonlinear damping σe^{κ} and turbulence energy flux Γ_e. Note that no closure approximation of Γ_e is necessary at this stage.

Assuming steady state and integrating Eq. 12 across the SOL in x direction, we obtain the key relation:

$$\Gamma_{e0} = \lambda_e\, |\gamma|\, e + \sigma\ e^{1+\kappa} \lambda_e \tag{13}$$

Here, Γ_{e0} is the intensity flux at the separatrix, $\gamma < 0$ is assumed, $\Gamma_e \to 0$ for large x, and e should be interpreted as a constant – the later is a layer averaged value. Note the intensity flux through the separatrix balances the linear and nonlinear damping of turbulent energy in the SOL. This equation will ultimately determine the layer width as a function of turbulence energy density e.

In the SOL, the linear growth rate is approximated by the following equation.

$$\gamma = \gamma_0 - \omega_s \tag{14}$$

It is justified by Fig 5, in the large shear limit, where the H-mode SOL sits. The nonlinear damping rate is σe^{κ}. The values of σ and κ vary between different saturation models. The sensitivity of the results to the assumptions concerning this model will be discussed in the later part of this paper.

The width of the SOL may be estimated:

$$\lambda = \lambda_e = \sqrt{\lambda_{HD}^2 + \tau^2 e} \tag{15}$$

Here, we calculate the root mean square of the radial distance travelled by a particle in the SOL before it is lost along the magnetic field, i.e. in time period $\tau = L_{\parallel}/c_s$, the parallel transit time. This distance is used as an estimate of the SOL width. Eq. 15 accounts for both magnetic drift v_D contribution, represented by the $\lambda_{HD} (\sim v_D \tau)$ term, and turbulent convection contribution. The turbulence is treated as a

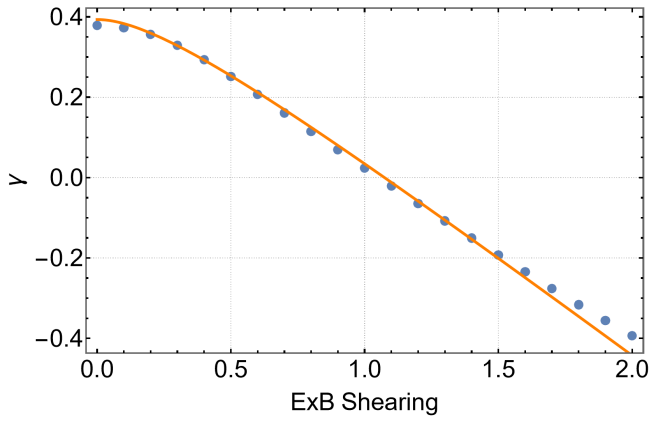

Figure 5: Linear Growth Rate of a specific mode (fixed k_y) v.s. $E \times B$ shear at $q = 5$, $\beta = 0.001$, $k_y \cdot \lambda_{HD} = 1.58$. The edge safety value q and $\beta = 2\rho_i/R$ are chosen based on experimentally relevant values. k_y is chosen so that the poloidal scale of the mode is of the same scale as the SOL, for which the mode is the most unstable.

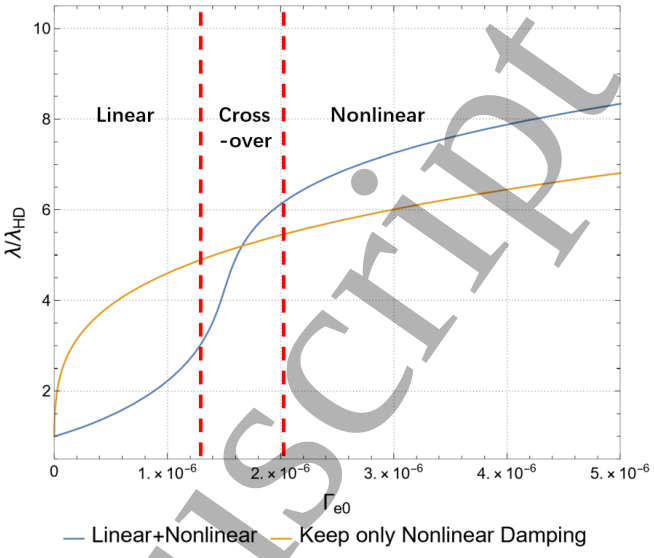

Figure 6: λ/λ_{HD} plotted against the intensity flux Γ_{e0} from the pedestal at $q = 4$, $\beta = 0.001, \kappa = 0.5$, $\sigma = 0.6$

stochastic process, thus explaining why the effects add in quadrature. The correlation time of the turbulence is assumed to be the parallel transit time, since parallel streaming is the main process in the SOL without turbulence. And it is still a good approximation when turbulence is weak, and so can be used as a first approximation when turbulence starts to have a broadening effect. *Note that the turbulent velocity needs to be comparable to the drift velocity v_D in order to have a significant influence on the width of the SOL. This ultimately sets the level of pedestal turbulence required, i.e. $e > v_D^2$.*

Combining Eq. 13, 14 and 15, the SOL width can be reduced to a function of Γ_{e0}, the intensity flux at the separatrix. A representative curve of λ/λ_{HD} v.s. Γ_{e0} is plotted in Fig. 6, where $\beta = 0.001, q = 4, \sigma = 0.6, \kappa = 0.5$. As the figure caption states, the curve can be divided into three regions. First, when the intensity flux is small, linear damping in the SOL dominates and balances Γ_{e0}. The SOL width then has a weak dependence on the intensity flux. When the intensity flux is large, the nonlinear damping dominates, so the SOL width increases slowly with Γ_{e0}. In between, there is a cross-over region, where damping and nonlinear damping are comparable. The linear damping reaches its maximal value in this region. In the cross-over region, the width of the SOL grows rapidly with increasing intensity flux Γ_{e0}. The prediction of the cross-over between linear and nonlinear regimes is a significant result of this paper.

Next, we need to relate Γ_{e0} to the pedestal turbulence, thus obtaining the minimal pedestal fluctuation level needed to cause significant SOL broadening. As will be discussed in the next section, this is determined by the value of Γ_{e0} required to enter the cross-over region.

4. SOL-Edge Connection II

In this section, the intensity flux Γ_0 is estimated in terms of pedestal parameters, and a scaling estimate of the pedestal fluctuation level needed to broaden the SOL is given.

The turbulence intensity flux in the pedestal can be approximated by the following coarse-grained expression:

$$\Gamma_{e0} = -\tau_c K \partial_x K \approx \tau_c K^2 / w_{ped} \qquad (16)$$

as illustrated by Fig. 7. Γ_e is the turbulence intensity flux from the pedestal to the SOL, and so encapsulates the crucial effect of turbulence spreading. Here, K is the turbulence kinetic energy density, τ_c is the correlation time of the turbulence in the pedestal and w_{ped} is the pedestal width, which here serves as an estimate for L_e, the scale length of pedestal turbulence intensity. Eq. 16 can be derived systematically in the weak turbulence limit [17] and can be generalized beyond that regime by considering different correlation times τ_c.

In turbulent pedestal, there are three classes of processes that can influence the correlation time:

(i) Linear growth rate or triad interaction time

(ii) Nonlinear decorrelation

(iii) $E \times B$ shearing

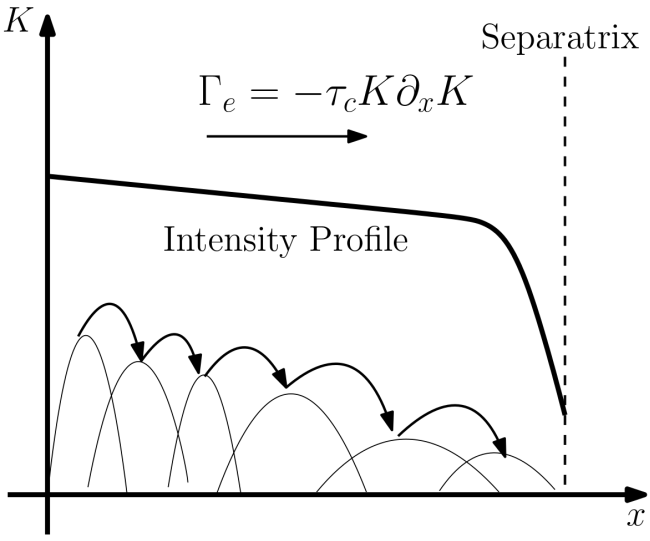

Figure 7: Turbulence Spreading in Pedestal

The first process is important in the weak turbulence regime, the second is important in the strong turbulence regime, while the third is important when the $E \times B$ Shearing rate is comparable to or larger than other rates. Of course, the last limit is the one of relevance here.

Since large $E \times B$ shear is characteristic of the pedestal, we first investigate the effect of $E \times B$ shearing on the decorrelation time. Shearing will decrease the intensity flux, as expected for a transport barrier[21]. A challenge here is for the pedestal intensity to be large enough for Γ_e to penetrate the transport barrier, but not so large as to excessively degrade confinement. Here we use the shear decorrelation rate to relate τ_c to D and ω_s[28]: D is the turbulent diffusion coefficient.

$$\tau_c^{-1} = Dk^2(1 + \omega_s^2 \tau_c^2) \tag{17}$$

The effective eddy size is modified by shearing, as illustrated in Fig. 8.

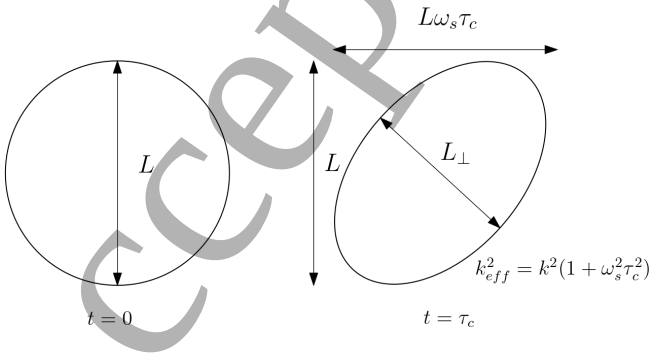

Figure 8: Shearing effects on eddy size and correlation length

In the strong shear limit:

$$\tau_c = \left(Dk^2\right)^{-1/3} \omega_s^{-2/3} \tag{18}$$

Then, using the Kubo formula[29] to relate D to the fluctuation level, we have:

$$\begin{aligned} D &= \int_0^\infty \langle v(0)\, v(\tau)\rangle d\tau \\ &= \int_0^\infty d\tau \sum_k |v_k|^2 e^{-k_y^2 \omega_s^2 D\tau^3 - k^2 D\tau} \end{aligned} \tag{19}$$

In the strong shear limit:

$$D \sim |v|^{1.5} k^{-0.5} \omega_s^{-0.5} \tag{20}$$

Combining the two steps above, we see that τ_c is related to ω_s and the fluctuation level in the strong shear limit as:

$$\tau_c = \tau_t^{0.5} \omega_s^{-0.5} \tag{21}$$

Here, τ_t is the eddy turnover rate: $\tau_t = 1/k|v|$. τ_t is also the correlation time of the turbulence when the $E \times B$ shear is weak. Therefore, Γ_{e0} is:

$$\Gamma_{e0} \sim \tau_t^{0.5} \omega_s^{-0.5} K \partial_x K \sim \tau_t^{0.5} \omega_s^{-0.5} K^2 / w_{ped} \tag{22}$$

The $E \times B$ shearing rate in the pedestal is estimated by radial force balance, so:

$$\omega_s \approx \partial_x \frac{\nabla p}{ne} \sim \frac{\rho^2}{w_{ped}^2} \Omega \tag{23}$$

Here, Ω is the ion gyro-frequency, ρ is the ion gyro-radius.

Now we apply the general estimation of the intensity flux above to the case of drift waves, taken as representative of micro-turbulence, and ballooning modes as representative of MHD turbulence or "Grassy ELMs". The goal here is to obtain estimates of the minimal pedestal fluctuation level needed to broaden the SOL. The minimal intensity flux needed is given by Eq. 13 and 15 as:

$$\Gamma_{e0\,min} = |\gamma| \lambda_{HD}^3 \tau_\parallel^{-2} \tag{24}$$

This estimate assumes that the velocity fluctuation $\tilde{v} \sim v_D$ i.e. the turbulent velocity becomes comparable to the magnetic drift velocity and linear damping dominates nonlinear damping when SOL width is of the same order of λ_{HD}. Thus, Eq. 24 gives an effective lower bound on the intensity flux needed to broaden the layer. The intensity flux from the pedestal then balances the linear damping of turbulence in the SOL. Note that this is the critical level of intensity flux required to enter the cross-over regime, as shown in Fig. 6.

4.1. Spreading of Micro-turbulence

Here, we apply the above general equation for intensity flux to micro-turbulence, as for drift waves. The correlation time for the drift wave turbulence, when the shearing is weak, is roughly:

$$\tau_{c0} v_* = \rho \tag{25}$$

Here, v_* is the drift velocity $c_s\rho/L_n$. L_n is the scale length of density gradient in the pedestal. This estimation of correlation time corresponds to the weak turbulence limit, and can be systematically derived using the TSDIA method[17].

Plugging Eq. 25 into Eq. 16 and 22, given that the wave length of the DW is of the order of ρ, we obtain the minimal pedestal fluctuation level needed to broaden the SOL in both the weak shear limit and strong shear limit. The results for the weak shear limit and the strong shear limit are:

Weak Shear Limit

$$\begin{aligned}\frac{|\delta v|}{c_s} &\sim \left(\frac{3L_e}{aL_n}\right)^{0.25} (\rho/R)^{0.5} q^{-0.25} \\ &\sim (\rho/R)^{0.5} q^{-0.25}\end{aligned} \tag{26}$$

Strong Shear Limit

$$\begin{aligned}\frac{|\delta v|}{c_s} &\sim \left(\frac{3L_e}{aL_n}\right)^{0.25} (\rho/R)^{0.5} q^{-0.25} \left(\frac{L_p}{\rho}\right)^{1/8} \\ &\sim (\rho/R)^{0.5} q^{-0.25} \left(\frac{w_{ped}}{\rho}\right)^{1/8}\end{aligned} \tag{27}$$

Here, L_e is the length scale of the turbulence profile in the pedestal, L_p is the pressure length scale in the pedestal, which is of the same order as L_n. These three scales are all estimated by pedestal width w_{ped}.

Notice that in both expressions, there is a factor of $(\rho/R)^{1/2} \approx (\rho_* L_{ped}/R)^{1/2}$ – a size-dependent, small coefficient. Here $\rho_* = \rho/L_{ped}$ is computed with the pedestal scale. Note the quite favorable size scaling of the required turbulence level. This indicates that the minimal fluctuation level needed is indeed small. Interestingly, Eq. 26 and 27 are similar, apart from the factor of $(w_{ped}/\rho)^{1/8}$. The ρ/R scaling also suggests that the critical levels of broadening can be achieved in larger devices with higher toroidal field.

Comparing the shearing rate and the correlation time τ_{c0}, we know that for small scale ($k \sim 1/\rho$) drift waves in pedestal, the $E \times B$ shearing is weak. Therefore, the weak shear limit should be used for the estimation for small scale drift waves

$$\omega_s \tau_{c0} = \rho/w_{ped} \tag{28}$$

Note that for larger scale drift waves, the strong shear form is relevant.

4.2. Spreading of MHD turbulence (Grassy ELMs)

Now we turn to MHD turbulence, as for the case of ballooning modes. This is related to turbulent pedestal regimes, such as states of Grassy ELMs.

Here, the growth rate of the ballooning mode is estimated by Eq.29, where L_{pc} represents the critical pedestal pressure gradient scale length which renders the ballooning mode marginally stable, ω_A is the Alfv́en frequency, $L_p \sim p/|\partial_x p|$. We have:

$$\gamma^2 = \omega_A^2 (L_{pc}/L_p - 1) \tag{29}$$

We take the correlation time as the linear growth time scale, which is valid when the MHD turbulence is weak (i.e. the case of interest).

$$\tau_{c0} = 1/\gamma \tag{30}$$

The correlation time is compared to the shearing rate in Eq.31. (w_{ped} is used to estimate L_p)

$$\omega_s \tau_{c0} = \frac{\sqrt{\beta_t} q \rho R}{w_{ped}^2 \sqrt{\frac{L_{pc}}{L_p} - 1}} \tag{31}$$

Since there are small parameters in both the numerator and the denominator, both weak shear and strong shear cases are possible, so both should be considered.

The turbulent velocity is estimated using the linear growth rate as:

$$\tilde{v} = \gamma \Delta_r \tag{32}$$

where Δ_r is the radial displacement of the mode. Plugging $K = \tilde{v}^2$ into Eq.16 and 22, we have the following scaling estimation of the supercriticality of the pedestal scale length needed to broaden the SOL (i.e. achieve the cross-over level, as discussed in the previous section). Note L_p/L_{pc} is on the left hand side, so Equations 33, 34 give a measure of super-criticality. We thus obtain:

Weak Shear Limit

$$\begin{aligned}\frac{L_{pc}}{L_p} - 1 &\sim (q\rho/R)^{4/3} \frac{R^2}{L_p^2} \frac{L_p^{8/3}}{\Delta_r^{8/3}} \beta_t \\ &\sim (q\rho/R)^{4/3} \frac{R^2}{w_{ped}^2} \frac{w_{ped}^{8/3}}{\Delta_r^{8/3}} \beta_t\end{aligned} \tag{33}$$

Strong Shear Limit

$$\begin{aligned}\frac{L_{pc}}{L_p} - 1 &\sim (q\rho/R)^{14/9} \frac{R^{8/3}}{L_p^{8/3}} \left(\frac{L_p}{\Delta_r}\right)^{16/9} \beta_t \\ &\sim (q\rho/R)^{14/9} \frac{R^{8/3}}{w_{ped}^{8/3}} \left(\frac{w_{ped}}{\Delta_r}\right)^{16/9} \beta_t\end{aligned} \tag{34}$$

Here, β_t is the toroidal beta.

In both scaling estimates, the required supercriticality scales with small parameters ρ/R and β_t. Therefore, the required super-criticality is quite small, corresponding to a pedestal state of MHD turbulence, such as the Grassy ELM regime. Thus, we see that a state of quasi-marginal ballooning turbulence is sufficient to achieve the cross-over level for SOL width broadening. And once again, we note a ρ/R scaling which is favorable for future devices.

5. Unified Estimation and Sensitivity Analysis

In this section, the results from the earlier two sections are combined to actually relate the width of the SOL to pedestal parameters, namely the pedestal fluctuation level for drift waves, and the supercriticality for ballooning turbulence. We will see that there is indeed a minimal fluctuation level or supercriticality needed to broaden the SOL beyond the HD prediction. The specific shape of the curves is sensitive to the nonlinear damping model. But a sensitivity analysis to various parameters of the nonlinear damping model is presented to show that the minimal fluctuation level is actually not sensitive to the specific nonlinear damping model and is determined mainly by the maximal value of the linear damping. These justify the scaling analysis of the minimal fluctuation level in the last section.

$$\Gamma_{e0} = |\gamma|\, e\lambda + \sigma e^{\kappa+1}\lambda \tag{35}$$

In order to do estimation, some scaling assumptions for σ(nonlinear damping coefficient) must be made. Here, σ is estimated by:

$$\sigma = a\,(\rho)^{-2\kappa}\left(\Omega\,(\rho/R)^{\alpha}\right)^{1-2\kappa} \tag{36}$$

The length scale for nonlinear damping is assumed to be ion gyro-radius ρ. This is an underestimation, and leads to an upper bound on σ. The time scale for nonlinear damping is chose to $\Omega\,(\rho/R)^{\alpha}$($\Omega$ is the gyro-frequency), $\alpha = 1$ for parallel transit time (which is an upper bound for the time scale), $\alpha = 0.5$ for ideal interchange growth, $\alpha = 0$ for gyro-frequency(which is an lower bound of the time scale). Here a is a dimensionless coefficient of $O\,(1)$. $\kappa = 1$ represents nonlinear damping for weak turbulence, $\kappa = 0.5$ represents nonlinear damping for strong turbulence. These arguments serve as guidelines for choosing the parameters in this section.

5.1. Typical Cases

In this subsection, cases with typical parameters are presented to relate the SOL width to pedestal fluctuation levels (for DW) and supercriticality (for ballooning). For all the cases, the following parameters are chosen. $\beta = 0.001$, $q = 4$, $\kappa = 0.5$, $\alpha = 0.5$, $a = 0.6$

For drift waves, the SOL width is determined as a function of the dimensionless mean electrostatic fluctuation level in the pedestal ($e\delta\phi/T$), as shown by the blue curve in Fig. 9. In addition, two other curves are plotted to show the relative importance of linear and nonlinear damping of turbulence in the SOL. These keep only the linear damping term or the nonlinear damping term in Eq. 35. The blue curve can be divided

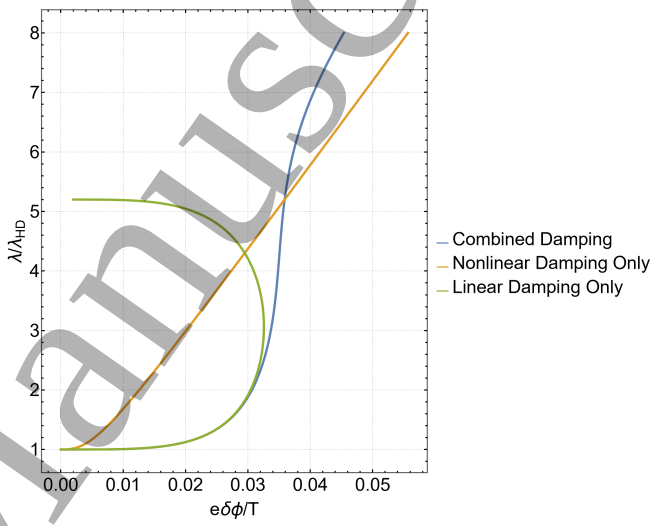

Figure 9: A typical Case for DW: the normalized pedestal width λ/λ_{HD} plotted against the normalized pedestal fluctuation level $e\delta\phi/T_e$

into three parts:

Linear Term Dominant This represents the part of the curve where $e\delta\phi/T < 0.03$ in Fig. 9. In this part, the linear damping dominates over the nonlinear damping, and the SOL width grows very slowly as $e\delta\phi/T$ increases.

Nonlinear Term Dominant This represents the part of the curve where $e\delta\phi/T > 0.04$ in Fig. 9. In this part, the nonlinear damping dominates over the linear damping. The curve bends downward, and the growth of the SOL width slows down as $e\delta\phi/T$ increases.

Cross-over Part This represents the part of the curve where $0.03 < e\delta\phi/T < 0.04$ in Fig. 9. In this part, the linear damping reaches its maximum. The nonlinear damping and linear damping are comparable. The SOL width grows rapidly as $e\delta\phi/T$ increases.

It is clear that the *minimal* pedestal fluctuation level needed to broaden the SOL is determined by the location of the cross over part of the curve. This in turn is determined by the maximal value of the linear

damping. In this case, the *minimal pedestal fluctuation level* needed is $\sim 0.03-0.05$, which is within the range of the fluctuation level for a turbulent pedestal[30]. We emphasize that the numerical values given here are approximations only. However, although this is only an estimate, it suggests that the SOL can be broadened without the need for unacceptably strong turbulence. The blue curve in Fig. 9 is one principal result of this paper.

The same procedure is repeated for ballooning modes with the same parameters in both the weak shear and strong shear limit, as shown in Fig. 10. The only difference is that the pedestal parameter is the supercriticality margin $L_{pc}/L_p - 1$. The general trend is similar. The curve can again be divided into 3 parts and the minimal supercriticality is indicated by the crossover region, and determined by the maximal linear damping in the SOL. For $\Delta_r/L_p = 0.5$, the estimated supercriticality is about 0.25 and so is relatively modest. This indicates that turbulent pedestals like those found in Grassy ELM regimes have the potential to support a wider SOL due to spreading, without much degradation of confinement.

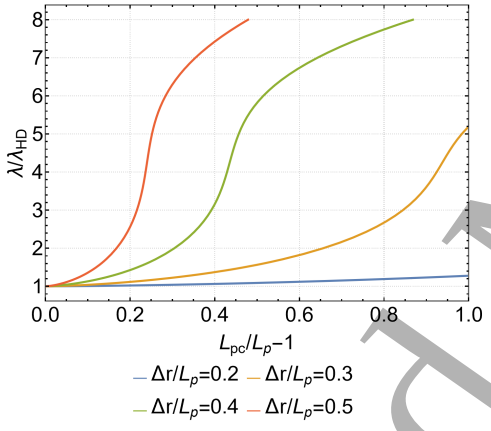

a) Weak Shear Case

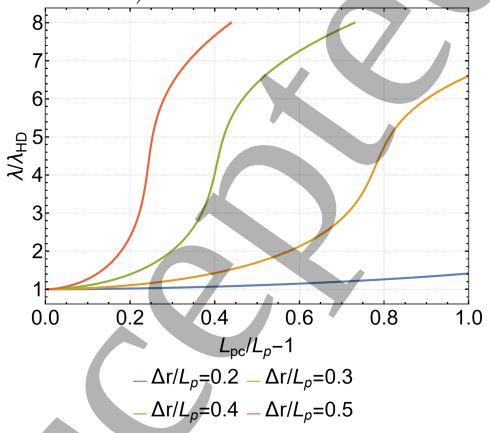

b) Strong Shear Case

Figure 10: Typical Cases for Ballooning. The normalized pedestal width λ/λ_{HD} is plotted against supercriticality $L_{pc}/L_p - 1$ at different mode width Δ/L_p

Next, we show that the existence of the minimal pedestal fluctuation level (or supercriticality) and that it is determined by the maximal linear damping in the SOL are both general results, and not due to the specific mechanism of nonlinear damping. These points are demonstrated by the sensitivity analysis in the following subsection.

5.2. Sensitivity Analysis

The sensitivity analysis is performed by giving different a, α, κ values for the curves "$e\delta\phi/T$(Pedestal) v.s. λ/λ_{HD}" and "$L_{pc}/L_p - 1$ (Pedestal) v.s. λ/λ_{HD}".

For drift waves, the results are presented in Fig. 11, 12 and 13. Note here the x and y coordinates have been swapped as compared with Fig. 9, in order to more effectively label the curves.

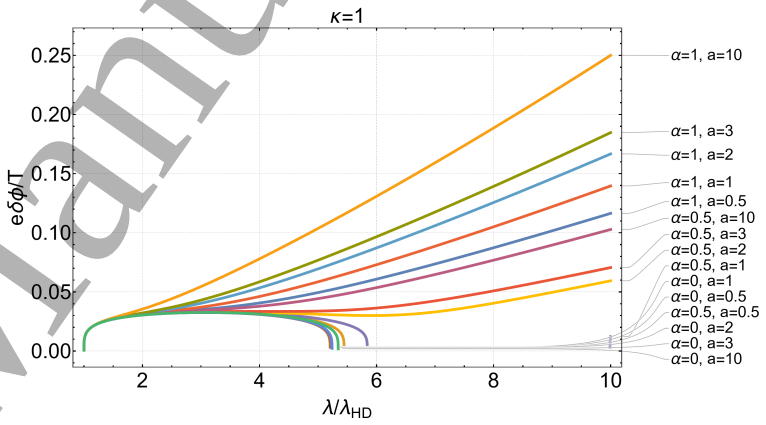

Figure 11: Sensitivity analysis of nonlinear model at $\kappa = 1$, $\beta = 0.001$, $q = 4$ for spreading of drift wave turbulence

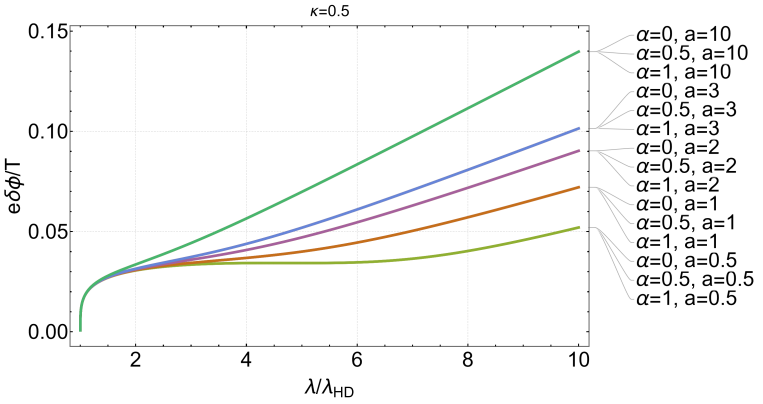

Figure 12: Sensitivity analysis of nonlinear model at $\kappa = 1/2$, $\beta = 0.001$, $q = 4$ for spreading of drift wave turbulence

Although the nonlinearly dominant region of the curves and the width of the cross-over region are

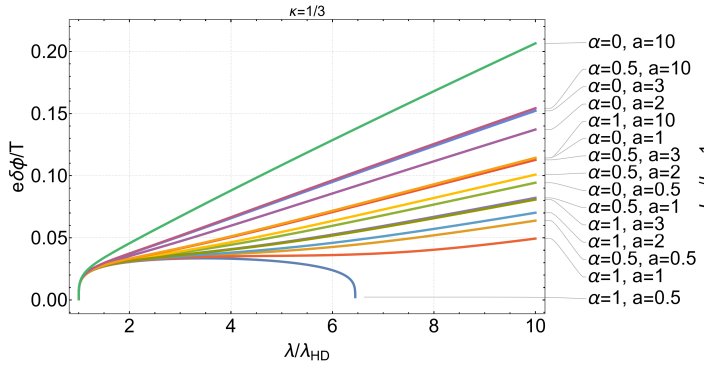

Figure 13: Sensitivity analysis of nonlinear model at $\kappa = 1/3$, $\beta = 0.001$, $q = 4$ for spreading of drift wave turbulence

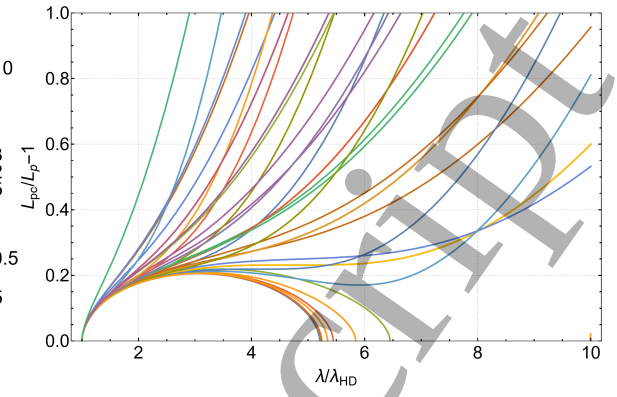

Figure 15: Sensitivity analysis of nonlinear model at $\beta = 0.001$, $q = 4$ for spreading of ballooning mode turbulence in strong weak limit

sensitive to the choice of the nonlinear damping model, all the curves have the same behavior in the linearly dominant region. The latter extends all the way to the start of the cross over region. There the SOL starts to be significantly broadened (The corresponding y value is the minimal fluctuation level needed). This shows that the existence of a minimal fluctuation level needed to broaden the SOL is a universal property, and that it is set by the maximal value of the linear damping.

For ballooning modes, the results are presented in Fig. 14 and 15. The x and y coordinates are also swapped as compared with the plots in the previous subsection. Again, all the curves have the same linearly dominant part. For most of the curves, the similarity continues to the start of the cross-over region. Therefore, the existence of a minimal fluctuation level needed to broaden the SOL, and the fact that this level is set by the maximal value of the linear damping, are also both insensitive to the nonlinear damping model.

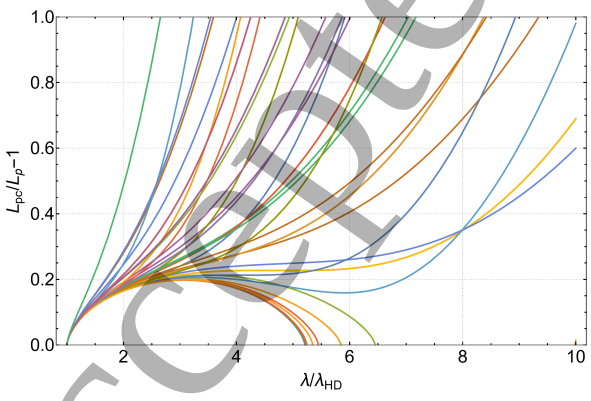

Figure 14: Sensitivity analysis of nonlinear model at $\beta = 0.001$, $q = 4$ for spreading of ballooning mode turbulence in weak shear limit $\kappa = 1, 1/2, 1/3$, $a = 0.5, 1, 2, 3, 5, 10$, $\alpha = 0, 0.5, 1$

6. Discussion

In this paper, we have developed the theory of the SOL scale, including the impact of turbulence spreading from the pedestal. In particular, we have derived a lower bound on the pedestal turbulence level required to broaden the SOL beyond the HD layer width. This effectively converts the SOL from a narrow laminar boundary layer to a broad turbulent boundary layer. The principal results of this paper are:

(i) The demonstration of the effects of strong stabilization of the SOL in the presence of large $E \times B$ shear stabilization and sheath boundary condition in H-mode. This finding is the underpinning of the success of the neoclassical HD model.

(ii) The use of a $K-\epsilon$ model to determine the pedestal turbulence level as a function of the turbulence intensity influx from the pedestal Γ_{e0}, and of SOL parameters. The principal competition is between Γ_{0e} and linear(shear) and nonlinear damping. The SOL width follows as $\lambda = \sqrt{\lambda_{HD}^2 + \tau^2 e}$. Fig. 6 shows the key result. Note the presence of two branches and a cross-over region, at which $\tilde{v}_{r\,rms} \sim v_D$. Achieving the cross-over is required to broaden the layer beyond the HD width. These results do not depend upon the microphysics of Γ_{0e}

(iii) The calculation for pedestal turbulence levels required to achieve significant layer broadening. The turbulence intensity flux is calculated in terms of pedestal parameters, including the $E \times B$ shear of the edge transport barrier. Two prototypical cases are studied – collisional drift waves (representative of microturbulence) and ballooning mode turbulence (representative of grassy ELMs). In the case of ballooning

turbulence, the analysis shows that a very weak supercriticality – consistent with a quasi-marginal state of 'grassy ELMs' – is necessary to broaden the layer. For drift wave turbulence, we show that relatively modest pedestal fluctuation levels of $e\delta\phi/T$ greater than a few percent are required for $\lambda/\lambda_{HD} > 2$, as shown in Fig. 9. The scalings of the minimal required $e\delta\phi/T$ and supercriticality are derived, and are strongly favorable with ρ/R.

(iv) A quantitative analysis of the sensitivity of the nonlinear damping model. This study shows that the existence of the cross-over region and the physics behind it – namely that the linear damping reaches a maximum – are not sensitive to the mechanism of the nonlinear damping. Thus, the competition between linear $E \times B$ shear damping and spreading from the core determines the critical condition for SOL broadening. This finding is a key result of this paper.

(v) The 'bottom line' that, taken together, items (i)-(iv) support the conclusion that a turbulent pedestal state of moderate fluctuation level can drive turbulence spreading sufficient to broaden the SOL heat load width well beyond the HD model prediction. Thus, a turbulent pedestal offers the possibility of two benefits, namely ELM mitigation and heat load broadening. This result boosts the attractiveness of such turbulent pedestal states, such as grassy ELM regimes, wide pedestal QH-mode and others.

We note here that two relatively recent simulation results suggest that SOL widths may broaden in the case of ITER parameters[31][32]. Turbulence spreading is invoked, but no analysis of either the dynamics of fluctuation intensity flux or the state of pedestal turbulence is given. The physics understanding offered is limited. We suggest that a direct measurement of the turbulence intensity flux across the separatrix should be implemented, and the scaling of the SOL width v.s. intensity flux should be explored. The dependence of the SOL width on pedestal turbulence levels is another topic for investigation.

We also suggest experimental studies to illuminate the key physics here. These should include a study of the SOL width scale in grassy ELM and wide pedestal QH states. Also, a study of how the SOL width responds to changes in ELM 'grassiness' (i.e. amplitude) would be of particular interest. Finally, we do not discuss possible back-spreading from SOL to the pedestal in this paper. Such a "tail wags the dog" process can occur when the SOL broadens so much as to turn off $E \times B$ shear stabilization.

More generally ,these results have several broader implications, which should be mentioned here. One, as noted above, is the observation that turbulent pedestal states offer a "two-for-one" benefit. Another is that the effect of turbulence spreading should be included in the energy balance which is used to calculate pedestal turbulence and transport, even in L-mode. Indeed, these are indications that the HD model does not explain all the data, even in H-mode[8]. Strong spreading is clearly a plus, as it regulates pedestal confinement while at the same time broadening the layer. Finally note that calculating the turbulence intensity flux entails understanding yet another cross-phase factor. Experiments should address the physics of the spreading phase factors, and how they compare to the familiar cross-phases for quadratic fluxes. To this end, we note that the spreading intensity flux Γ_e, say $\sim \langle \tilde{v}_r \tilde{n}^2 \rangle$, is necessarily a triplet, as compared to the familiar particle, etc. fluxes ($\Gamma_n \sim \langle \tilde{v}_r \tilde{n} \rangle$), which are quadratic. Thus the spreading flux is a consequence of nonlinear triad interactions, as apposed to simple quasilinear processes. Bicoherence analysis of the spreading dynamics should be pursued, so as to illuminate the basic physics of turbulence spreading. This is essential to understanding the physics underpinnings of SOL broadening.

Acknowledgments

We thank Rob Goldston, Ting Wu, Jose Boedo, Chris McDevitt, Qinghao Yan, Ting Long, Xueqiao Xu and Nami Li for helpful discussions, and Jose Boedo for a critical reading of the manuscript. Stimulating interactions with participants in the 2021 Virtual Festival de Theorie are acknowledged. Xu Chu thanks Peking University for its hospitality while some of the work was performed there. This research was supported by US DOE under Award No. DE-FG02-04ER54738.

[1] Kikuchi M, Takizuka T, Medvedev S, Ando T, Chen D, Li J X, Austin M, Sauter O, Villard L, Merle A, Fontana M, Kishimoto Y and Imadera K 2019 *Nuclear Fusion* **59** 056017 ISSN 0029-5515

[2] Wagner F, Becker G, Behringer K, Campbell D, Eberhagen A, Engelhardt W, Fussmann G, Gehre O, Gernhardt J, Gierke G v, Haas G, Huang M, Karger F, Keilhacker M, Klüber O, Kornherr M, Lackner K, Lisitano G, Lister G G, Mayer H M, Meisel D, Müller E R, Murmann H, Niedermeyer H, Poschenrieder W, Rapp H, Röhr H, Schneider F, Siller G, Speth E, Stäbler A, Steuer K H, Venus G, Vollmer O and Yü Z 1982 *Physical review letters* **49** 1408–1412 ISSN 0031-9007

[3] Wootton A J, Carreras B A, Matsumoto H, McGuire K, Peebles W A, Ritz C P, Terry P W and Zweben S J 1990 *Physics of Fluids B: Plasma Physics* **2** 2879–2903 ISSN 0899-8221

[4] Landau L D and Lifshiñtśs E M 1987 *Course of theoretical physics. Vol 6, Fluid mechanics* 2nd ed (Oxford: Pergamon) ISBN 0080339336

[5] Townsend A A 1976 *The structure of turbulent shear flow* 2nd ed Cambridge monographs on mechanics and applied mathematics (Cambridge: Cambridge University Press) ISBN 052120710X

[6] Eich T, Leonard A W, Pitts R A, Fundamenski W, Goldston R J, Gray T K, Herrmann A, Kirk A, Kallenbach A, Kardaun O, Kukushkin A S, LaBombard B, Maingi R, Makowski M A, Scarabosio A, Sieglin B, Terry J and Thornton A 2013 *Nuclear Fusion* **53** 093031 ISSN 0029-5515

[7] Goldston R J 2011 *Nuclear Fusion* **52** 013009 ISSN 0029-5515

[8] Silvagni D, Eich T, Faitsch M, Happel T, Sieglin B, David P, Nille D, Gil L and Stroth U 2020 *Plasma Physics and Controlled Fusion* **62** 045015 ISSN 0741-3335

[9] Zhang Y, Krasheninnikov S I and Smolyakov A I 2020 *Physics of Plasmas* **27** 020701 ISSN 1070-664X

[10] Hahm T S and Diamond P H 2018 *Journal of the Korean Physical Society* **73** 747–792 ISSN 0374-4884

[11] Chen X, Burrell K H, Osborne T H, Solomon W M, Barada K, Garofalo A M, Groebner R J, Luhmann N C, McKee G R, Muscatello C M, Ono M, Petty C C, Porkolab M, Rhodes T L, Rost J C, Snyder P B, Staebler G M, Tobias B J and Yan Z 2017 *Nuclear Fusion* **57** 022007 ISSN 0029-5515

[12] Nazikian R, Petty C C, Bortolon A, Chen X, Eldon D, Evans T E, Grierson B A, Ferraro N M, Haskey S R, Knolker M, Lasnier C, Logan N C, Moyer R A, Orlov D, Osborne T H, Paz-Soldan C, Turco F, Wang H Q and Weisberg D B 2018 *Nuclear Fusion* **58** 106010 ISSN 0029-5515

[13] Wu T, Xu M, Nie L, Yu Y, Xu J, Long T, He Y, Cheng J, Yan L, Huang Z, Ke R, Shi P, Wang S and Liu B 2021 *Plasma Science and Technology* **23** 025101 ISSN 1009-0630

[14] Estrada T, Hidalgo C and Happel T 2011 *Nuclear Fusion* **51** 032001 ISSN 0029-5515

[15] Manz P, Ribeiro T T, Scott B D, Birkenmeier G, Carralero D, Fuchert G, Müller S H, Müller H W, Stroth U and Wolfrum E 2015 *Physics of Plasmas* **22** 022308 ISSN 1070-664X

[16] Grenfell G, van Milligen B, Losada U, Estrada T, Liu B, Silva C, Spolaore M and Hidalgo C 2020 *Nuclear Fusion* **60** 014001 ISSN 0029-5515

[17] Gürcan Ö D, Diamond P H and Hahm T S 2006 *Physics of Plasmas* **13** 052306 ISSN 1070-664X

[18] Garbet X, Laurent L, Samain A and Chinardet J 1994 *Nuclear Fusion* **34** 963–974 ISSN 0029-5515

[19] Manz P, Xu M, Fedorczak N, Thakur S C and Tynan G R 2012 *Physics of Plasmas* **19** 012309 ISSN 1070-664X

[20] Gürcan Ö D, Diamond P H, Hahm T S and Lin Z 2005 *Physics of Plasmas* **12** 032303 ISSN 1070-664X

[21] Wang W X, Hahm T S, Lee W W, Rewoldt G, Manickam J and Tang W M 2007 *Physics of Plasmas* **14** 072306 ISSN 1070-664X

[22] Brunner D, Kuang A Q, LaBombard B and Terry J L 2018 *Nuclear Fusion* **58** 076010 ISSN 0029-5515

[23] Zweben S J, Boedo J A, Grulke O, Hidalgo C, LaBombard B, Maqueda R J, Scarin P and Terry J L 2007 *Plasma Physics and Controlled Fusion* **49** S1–S23 ISSN 0741-3335

[24] D'Ippolito D A, Myra J R and Krasheninnikov S I 2002 *Physics of Plasmas* **9** 222–233 ISSN 1070-664X

[25] Garbet X, Sarazin Y, Imbeaux F, Ghendrih P, Bourdelle C, Gürcan Ö D and Diamond P H 2007 *Physics of Plasmas* **14** 122305 ISSN 1070-664X

[26] Hahm T S, Diamond P H, Lin Z, Itoh K and Itoh S I 2004 *Plasma Physics and Controlled Fusion* **46** A323–A333 ISSN 0741-3335

[27] Yan Q and Diamond P H 2021 *Plasma Physics and Controlled Fusion* **63** 085017 ISSN 0741-3335

[28] Biglari H, Diamond P H and Terry P W 1990 *Physics of Fluids B: Plasma Physics* **2** 1–4 ISSN 0899-8221

[29] Kubo R 1957 *Journal of the Physical Society of Japan* **12** 570–586 ISSN 0031-9015

[30] Boedo J A, Myra J R, Zweben S, Maingi R, Maqueda R J, Soukhanovskii V A, Ahn J W, Canik J, Crocker N, D'Ippolito D A, Bell R, Kugel H, Leblanc B, Roquemore L A and Rudakov D L 2014 *Physics of Plasmas* **21** 042309 ISSN 1070-664X

[31] Xu X Q, Li N M, Li Z Y, Chen B, Xia T Y, Tang T F, Zhu B and Chan V S 2019 *Nuclear Fusion* **59** 126039 ISSN 0029-5515

[32] Chang C S, Ku S, Loarte A, Parail V, Köchl F, Romanelli M, Maingi R, Ahn J W, Gray T, Hughes J, LaBombard B, Leonard T, Makowski M and Terry J 2017 *Nuclear Fusion* **57** 116023 ISSN 0029-5515